scientific reports

Check for updates

OPEN

Transcriptomic and proteomic integrated analysis reveals molecular mechanisms of 3D bioprinted vaginal scaffolds in vaginal regeneration

Xuemei Zhang[1,2], Jiahua Zheng[1], Liye Zhang[3], Jingkun Zhang[1], Li Feng[4], Lin Zhang[1]✉ & Xianghua Huang[1]✉

3D Bioprinting technology has been applied to vaginal reconstruction with satisfactory results. Understanding the transcriptome and proteome of regenerated vaginas is essential for knowing how biomaterials and seed cells contribute to vaginal regeneration. There are no reports on the systemic analysis of vaginal regeneration transcriptomes or proteomes. This study aims to explore the transcriptomic and proteomic features of vaginal tissue reconstructed with 3D bioprinted scaffolds. The scaffolds were made with biomaterials and bone marrow-derived mesenchymal stem cells (BMSCs) and then transplanted into a rabbit model.rna sequencing was used to analyze the transcriptomes of reconstructed and normal vaginal tissues, identifying 11,956 differentially expressed genes (DEGs). Proteomic analysis using liquid chromatography-tandem mass spectrometry (LC-MS/MS) and data-independent acquisition (DIA) identified 7,363 differentially expressed proteins (DEPs). Gene ontology (GO) and Kyoto encyclopedia of genes and genomes (KEGG) enrichment analyses were performed on DEGs and deps. Results showed that DEGs and deps.were involved in extracellular matrix remodeling, angiogenesis, inflammatory response, epithelialization, and muscle formation. This study shows that 3D bioprinted scaffolds are feasible for vaginal reconstruction and offers new insights into the molecular mechanisms involved.

Keywords Vaginal reconstruction, Biological scaffold, Bone marrow-derived mesenchymal stem cells, Proteomics, Transcriptomics

The vagina is a key part of the female reproductive system and is important for sexual health and reproduction. Congenital defects, trauma, or diseases can cause vaginal deformities, requiring either non-surgical or surgical treatments for reconstruction[1]. While traditional reconstruction methods (e.g., autologous grafts) remain clinically relevant, they frequently lead to complications such as graft contraction, sensory deficits, and reduced biocompatibility, significantly impacting patients' quality of life[2]. Recent breakthroughs in tissue engineering have opened transformative avenues for vaginal repair. Bioengineered implants designed to mimic the native extracellular matrix (ECM) now offer unprecedented opportunities to address these limitations[3]. ECM scaffolds derived from tissue-specific decellularized matrices are particularly advantageous, as they retain organ-specific ultrastructure and bioactive cues to guide cell migration, adhesion, and spatial organization[4]. To enhance functional performance, hybrid bioinks combining ECM with photocrosslinkable polymers like gelatin methacryloyl (GelMA) and silk fibroin (SF) have been developed, synergistically improving mechanical resilience, printability, and pro-regenerative signaling[5,6].

However, replicating the vagina's intricate multilayered architecture—comprising stratified epithelium, vascularized connective tissue, and smooth muscle bundles—remains a formidable challenge[7]. Bone marrow-

[1]Department of Obstetrics and Gynecology, The Second Hospital of Hebei Medical University, 215 Heping West Road, Shijiazhuang 050000, Hebei Province, China. [2]Department of Pelvic floor clinic, Cangzhou Central Hospital, Cangzhou 061600, Hebei Province, China. [3]Chengde Medical University, Chengde 067000, Hebei Province, China. [4]Department of Gynecology, The Fourth Hospital of Shijiazhuang, Shijiazhuang 050000, Hebei Province, China. ✉email: 28101738@hebmu.edu.cn; huangxh2022@hebmu.edu.cn

derived mesenchymal stem cells (BMSCs) are promising because they can renew themselves, differentiate into various cell types, modulate immune responses, promote tissue remodeling, and act as seeding cells in vaginal reconstruction[8,9]. Recent studies further highlight the therapeutic potential of engineered MSCs in vascular and muscular regeneration. For instance, long-term exposure to stromal cell-derived factor-1α (SDF-1α) secreted by genetically modified MSCs has been shown to enhance vascular regeneration and skeletal muscle repair in ischemic hindlimb models, demonstrating their capacity to orchestrate microenvironmental cues critical for complex tissue regeneration[10].

Tissue regeneration is governed by dynamic interactions between cells, biomaterials, and biochemical signals—a process encompassing inflammation resolution, ECM remodeling, and coordinated angiogenesis[11]. While small defects may heal spontaneously, extensive injuries often culminate in fibrotic scarring or functional impairment, highlighting the need for biomaterial-guided regenerative strategies[12]. The ECM's role extends beyond structural support; its tissue-specific composition (collagens, fibronectin, proteoglycans) establishes biochemical and biomechanical niches that regulate cellular behavior and fate[13]. Cell therapy currently holds a leading position in tissue engineering and regenerative medicine. MSCs secrete bioactive factors like soluble proteins, lipids, nucleic acids, and extracellular vesicles, which have anti-inflammatory, anti-scar, immune-regulatory, and anti-apoptotic properties[14]. By leveraging organ-specific ECM scaffolds alongside stem cell technologies, researchers can better emulate native tissue microenvironments to promote functional integration.

Our recent study suggests that personalized 3D bioprinted biomimetic scaffolds could be a viable option for restoring damaged vaginal structure and function[15]. This technology fabricates personalized vaginal implants by creating bioinks from decellularized animal-derived vaginal tissue, recellularizing them with allogeneic BMSCs, and employing 3D bioprinting for anatomical precision. Our findings demonstrate that 3D-bioprinted scaffolds—whether acellular or BMSC-laden—achieve in vivo cellularization and vascular integration. However, BMSC-seeded constructs exhibit superior structural regeneration, including enhanced epithelial stratification and smooth muscle alignment, underscoring the synergy between biomimetic scaffolds and cellular therapy. To elucidate these mechanisms, we conducted the first integrated transcriptomic-proteomic analysis of vaginal reconstruction, identifying critical pathways (ECM remodeling, angiogenesis) that govern scaffold-mediated regeneration. This work establishes a foundational framework for developing patient-specific regenerative solutions.

Results

Construction and in situ transplantation of 3D bioengineered vaginal scaffolds

P3 - BMSCs, when observed under an inverted phase contrast microscope, exhibited a uniform elongated morphology (Fig. 1A). These cells were then encapsulated within the ECM - GelMA - SF bioink (Fig. 1B) and loaded into a 3D bioprinter syringe. Subsequently, a 3D bioengineered scaffold was fabricated according to pre - set parameters (Fig. 1C). After 7 days of in vitro culture, live - dead cell staining results demonstrated the presence of numerous green live cells, indicating robust cell growth within the scaffold (Fig. 1D). A New Zealand rabbit vaginal defect model was successfully established, and the prepared scaffold was transplanted in situ without complications (Fig. 1E).

Histological staining of reconstructed vaginal tissues

Twelve weeks post - in situ transplantation of the scaffolds, samples of the reconstructed vaginal tissues were collected. Gross examination of these tissues revealed a well - developed vascular network, smooth mucosa, and prominent folds. The texture was resilient and elastic, closely resembling that of normal vaginal tissue, with

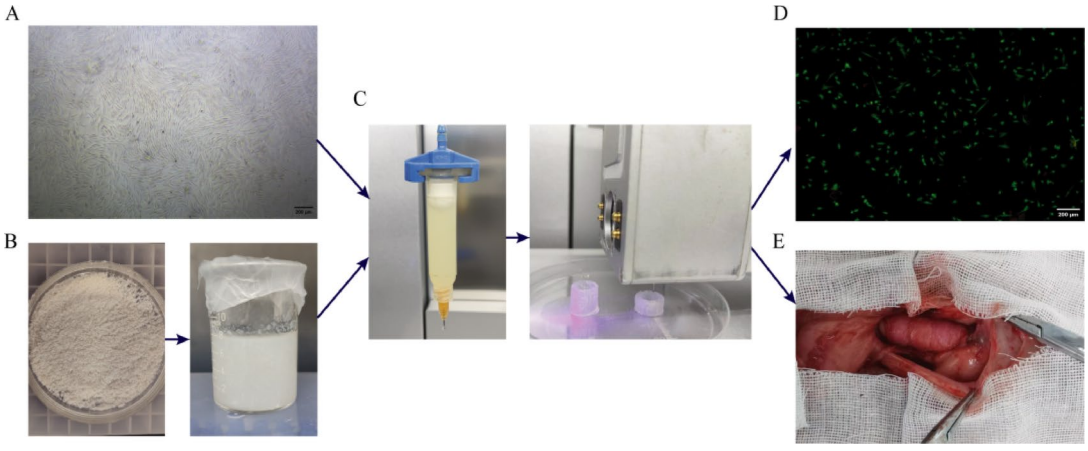

Fig. 1. The process of 3D printing and orthotopic transplantation of vaginal biomimetic scaffold. (**A**) The morphology of BMSCs at the P3. Scale bar 200 μm. (**B**) Porcine vaginal ECM powder and vECM-GelMA-SF hydrogel. (**C**) The process of bioink loading and 3D bioprinted vaginal biomimetic scaffold. (**D**) Staining of live/dead cells from biomimetic scaffolds encasing BMSCs after 7 days in vitro culture. Scale bar 200 μm. (**E**) The orthotopic transplantation process of rabbit vagina.

the 3D cell - bioengineered scaffold group showing the most promising results (Fig. 2). Histological analysis using HE staining revealed a well - organized epithelial structure with distinct folds in normal vaginal tissue. In both reconstructed vaginal tissue groups, epithelial cells were present 12 weeks after transplantation. However, in the 3D cell - bioengineered scaffold group, the epithelial cells were plump, regularly arranged, and formed prominent mucosal folds. The submucosal tissue beneath the epithelium was loose and rich in blood vessels and collagen fibers, closely mimicking the normal tissue structure, with no significant differences noted compared to normal tissue. In contrast, the 3D cell - free bioengineered scaffold group had thin and sparse epithelial layers with irregular cell arrangements. Periodic acid - Schiff (PAS) staining confirmed glycogen synthesis in the newly formed epithelial cells. Purple - red positive cells were observed in both normal and reconstructed vaginal epithelium, with more intense staining in the 3D cell - bioengineered scaffold group compared to the 3D cell - free bioengineered scaffold group. Masson's trichrome and Van Gieson (VG) staining showed a smooth muscle layer beneath the normal vaginal mucosa, with an inner circular and outer longitudinal arrangement of blood vessels and collagen fibers. In both reconstructed vaginal tissue groups, numerous blood vessels were present in the submucosal fibers, and muscle fibers (appearing red in Masson and yellow in VG) surrounded the vessel walls. In the 3D cell - bioengineered scaffold group, the muscle fibers were regularly arranged and dense, closely resembling the smooth muscle fibers in normal vaginal tissue (Fig. 2).

Analysis of differentially expressed genes (DEGs)

To investigate the impact of different bioengineered scaffolds on vaginal regeneration, gene activity was analyzed in normal vaginal tissue (N), 3D cell - free biomimetic scaffolds (Z), and 3D cell - loaded biomimetic scaffolds (C). Genes from each sample were statistically analyzed, and UpSet plots were generated to display the unique and common gene expressions among the groups (Fig. 3A). Gene expression levels were normalized using FPKM for comparison across different genes and samples (Fig. 3B). The correlation analysis of gene expression levels between samples was conducted to verify experimental reliability. The results showed strong correlations (above 0.8) within each group, indicating high experimental reliability (Fig. 3C). Principal component analysis (PCA) effectively grouped similar samples together, with closer distances between samples signifying higher similarity (Fig. 3D). This analysis confirmed that the sample grouping based on gene expression profiles was consistent and robust.

Differential expression gene (DEG) analysis

DEG analysis was performed to explore how different bioengineered scaffolds regulate vaginal regeneration by comparing groups N, C, and Z. Among the 11,956 annotated genes, the C group had 7,249 DEGs compared to N, with 4,023 genes upregulated and 3,226 genes downregulated. The Z group exhibited 6,684 DEGs, including 3,374 upregulated and 3,310 downregulated genes. When comparing C to Z, 5,960 DEGs were identified, with 3,607 genes upregulated and 2,353 genes downregulated (Fig. 4A). Volcano plots (Fig. 4B–D) visually represented the distribution of DEGs. A Venn diagram (Fig. 4E) illustrated the overlap of DEGs among the comparison groups. There were 1,467 DEGs common to all three comparison groups, and 2,595 DEGs unique to the C - N and Z - N comparisons. These DEGs may play crucial roles in understanding how different treatments regulate vaginal tissue regeneration. Cluster heatmaps (Fig. 4F) depicted the gene expression patterns and clustering relationships among the genes and samples. The results clearly showed separation and color differences among the N, C, and Z groups, indicating significant differences in gene expression patterns. However, samples within each group were closely clustered, suggesting similar gene expression patterns within each treatment group.

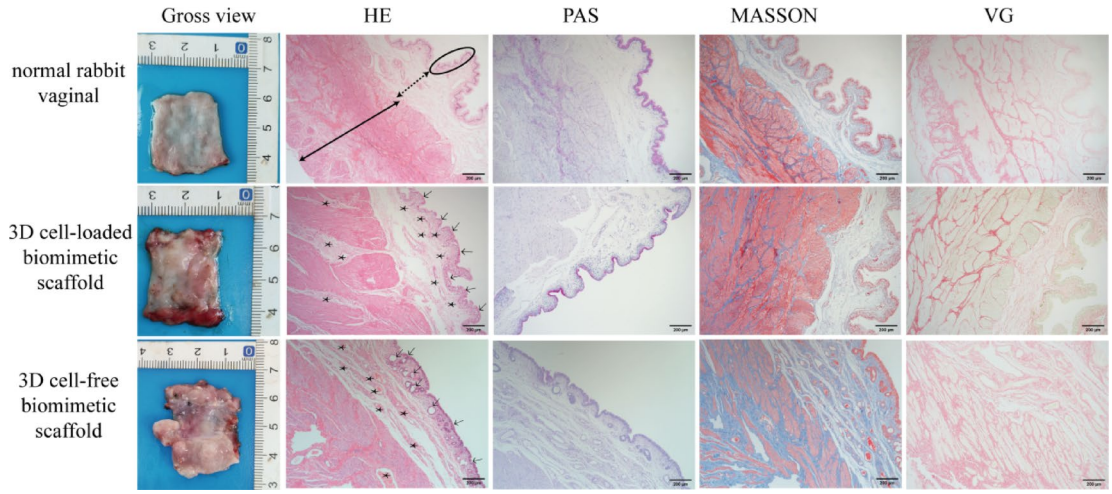

Fig. 2. After 12 weeks, gross view after specimen collection, HE staining, PAS staining, Masson's trichrome staining and VG staining of newly formed vaginas each group. The smooth muscle layer, subepithelial connective tissue, and epithelial layer are demarcated by solid lines, dashed lines, and circles, respectively. Regenerated blood vessels are labeled with asterisks (*), and the epithelium is indicated by arrows (→). Scale bar 200 μm.

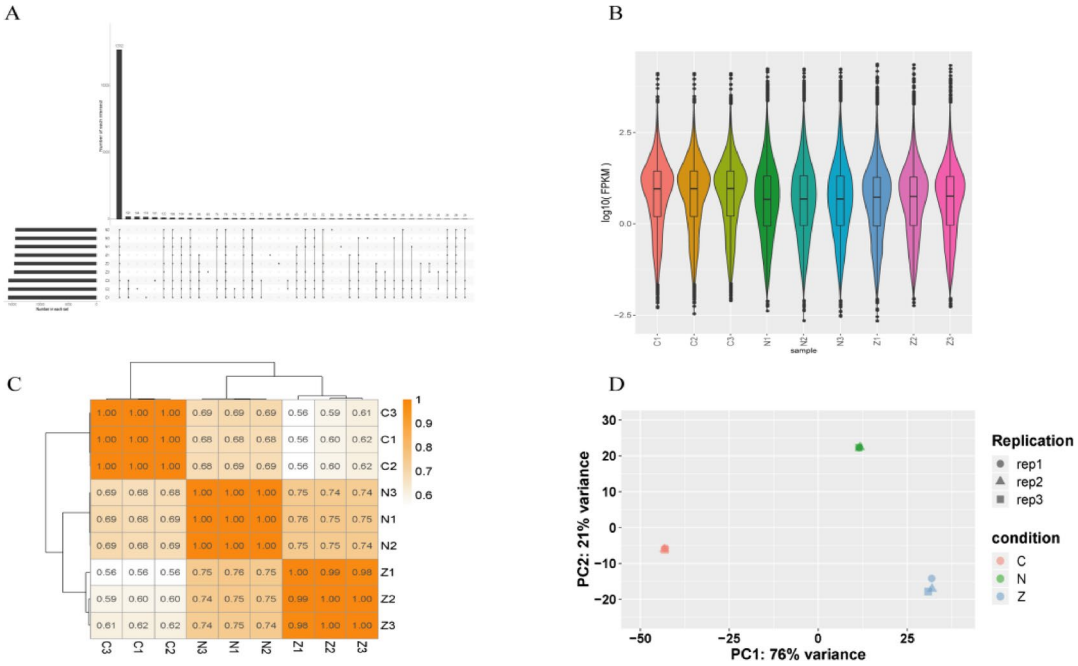

Fig. 3. Analysis of gene expression in each group includes: (**A**) The gene UpSet map for each sample identification, (**B**) The FPKM density distribution map, (**C**) The sample correlation test, with colored squares showing correlation levels between samples, (**D**) PCA analysis, where different shapes represent samples and different colors indicate groupings.

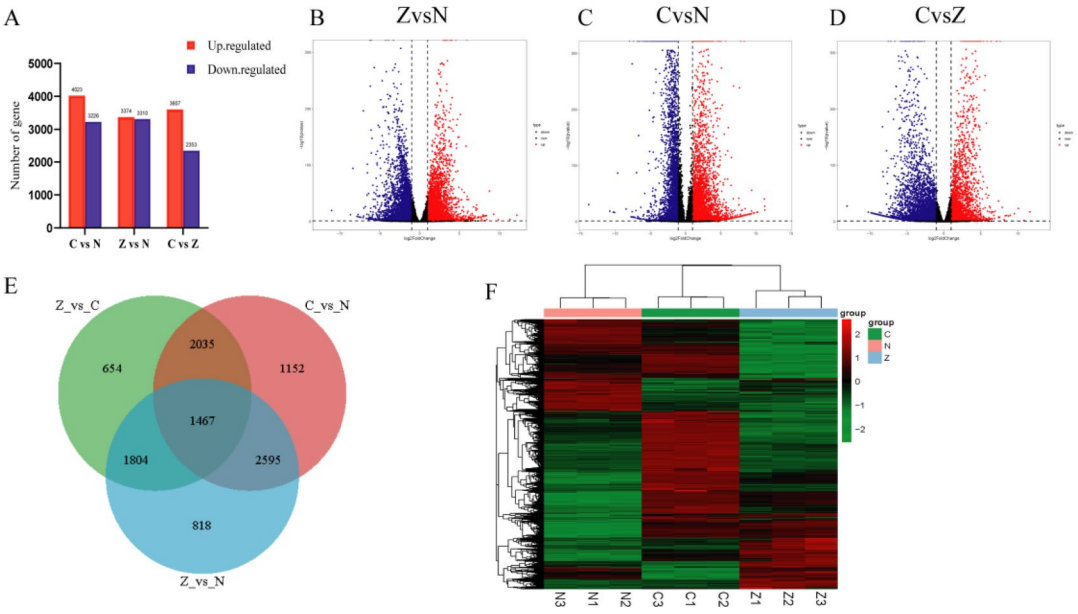

Fig. 4. Analysis of gene differential expression in the three sample groups includes: (**A**) A bar graph showing the results of differential expression analysis, (**B**–**D**) Volcano plots for differentially expressed genes in the CvsN, ZvsN, and CvsZ comparisons, with the x-axis representing log2FoldChange and the y-axis representing -log10(p-value); up-regulated genes are shown in red and down-regulated genes in blue, (**E**) Venn diagrams illustrating shared and unique differential genes between the comparison groups, (**F**) A heatmap of clustered differentially expressed genes, with highly expressed genes shown in red and low-expressed genes in green.

Analysis of differentially expressed proteins (DEPs)

To understand the influence of different bioengineered scaffolds on vaginal regeneration at the protein level, proteomic analysis was carried out. PCA clustered similar samples together, with closer distances between samples indicating higher similarity (Fig. 5A), which confirmed the reliability of protein levels and the appropriateness of sample selection (Fig. 5B). A total of 7,363 proteins were identified as differentially expressed across all groups. Compared to N, the Z group had 460 DEPs, with 270 upregulated and 190 downregulated proteins. The C group had 557 DEPs, with 454 upregulated and 103 downregulated proteins. When comparing C to Z, 496 DEPs were found, with 367 upregulated and 129 downregulated proteins. The volcano plot (Fig. 5C) showed the distribution of DEPs among the groups. A heatmap (Fig. 5D) presented the hierarchical clustering analysis of DEPs from the three comparison groups. The heatmap demonstrated that DEPs meeting the fold - change criteria (> 2) and statistical significance ($p < 0.05$) effectively separated the comparison groups, validating the selection of DEPs.

Protein-protein interaction (PPI) network analysis

Proteins do not function in isolation; their activities rely on interactions with other proteins and regulatory mechanisms. Combining PPI network analysis with pathway annotation provides a detailed model of cellular activities, facilitating the exploration of molecular mechanisms. Figure 6A shows the PPI network constructed from the DEPs of the three comparison groups. Further analysis identified the top 30 DEPs with the highest connectivity, which were highlighted in the PPI network graph (Fig. 6B). This approach helped identify key proteins and revealed their interactions within biological systems, offering insights into their roles and potential impact on vaginal tissue regeneration.

Gene ontology (GO) enrichment analysis

GO enrichment analysis was performed on the top 30 key proteins from each comparison group to clarify their functional roles. In the Z - N comparison group, key proteins were significantly enriched in processes such as cell migration, regulation of cell shape, cell adhesion, positive regulation of translation, peptide cross - linking, acute - phase response, and tissue homeostasis. These proteins were enriched in cellular components like the extracellular region, extracellular space, stress fibers, intermediate filaments, and the lateral plasma membrane. They were involved in functions such as heparin binding, calcium - dependent protein binding, integrin binding, and fibronectin binding. In the C - N comparison group, key proteins were mainly associated with biological processes including cell adhesion, acute - phase response, integrin - mediated signaling pathway, protein polymerization, response to calcium ion, adaptive immune response, and platelet activation. The enriched cellular components included the extracellular region, collagen trimer, phagocytic vesicle, basement membrane, focal adhesion, and endoplasmic reticulum exit site. These proteins participated in molecular functions such as heparin binding, fibronectin binding, collagen binding, integrin binding, extracellular matrix structural constituent, and signaling receptor binding. In the C - Z comparison group, key proteins were significantly enriched in biological processes such as complement activation, acute - phase response, platelet activation, positive regulation of phagocytosis, and blood coagulation. They were predominantly localized to the extracellular space and cell surface. These proteins were involved in molecular functions including heparin binding, fibronectin binding, collagen binding, antioxidant activity, laminin binding, and calcium ion binding (Fig. 7A).

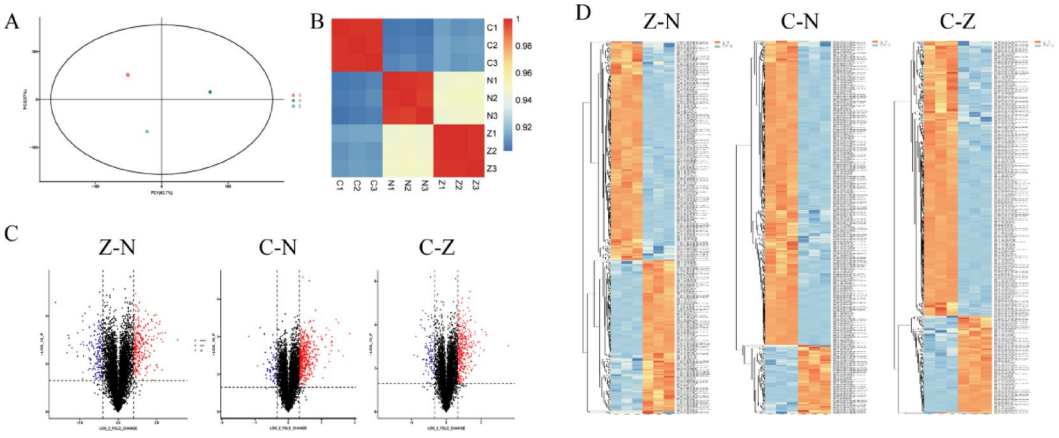

Fig. 5. Proteomic results for reconstructed and normal vaginal tissues include: (**A**) PCA analysis, with different shapes representing samples and colors indicating groupings, (**B**) Sample correlation test, where colored squares show high or low correlations between samples, (**C**) Volcano plot of DEPs for the three comparison groups, (**D**) Heatmap of hierarchical clustering analysis for DEPs across the three comparison groups.

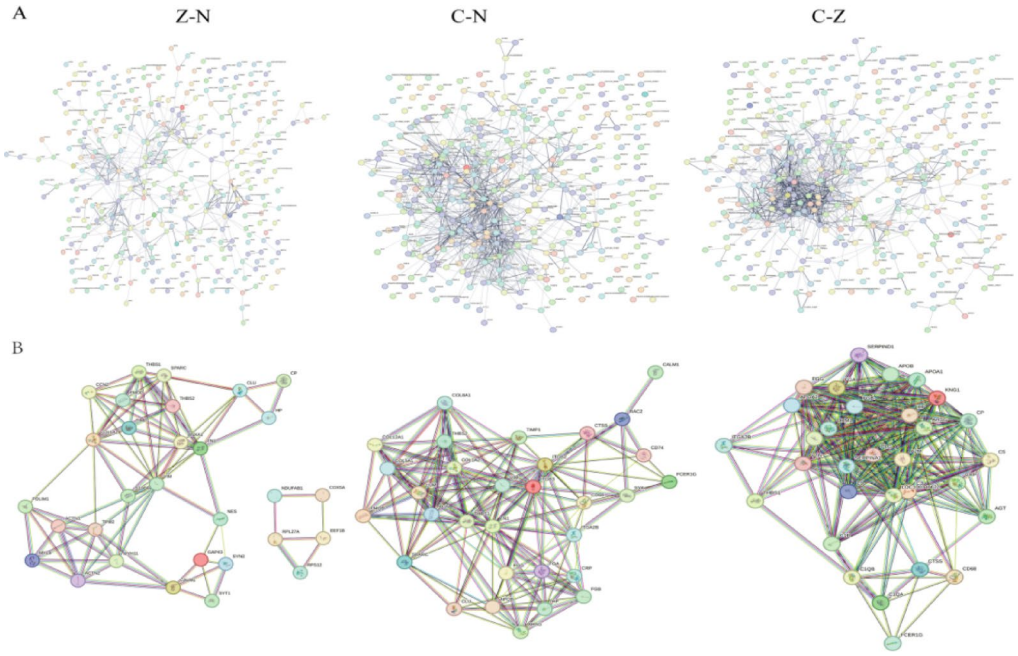

Fig. 6. PPI network plots of DEPs between the three comparison groups. (**A**) all DEPs for the three comparison groups: C vs. N, C vs. Z, and Z vs. N. (**B**) The top 30 DEPs for C vs. N, C vs. Z, and Z vs. N.

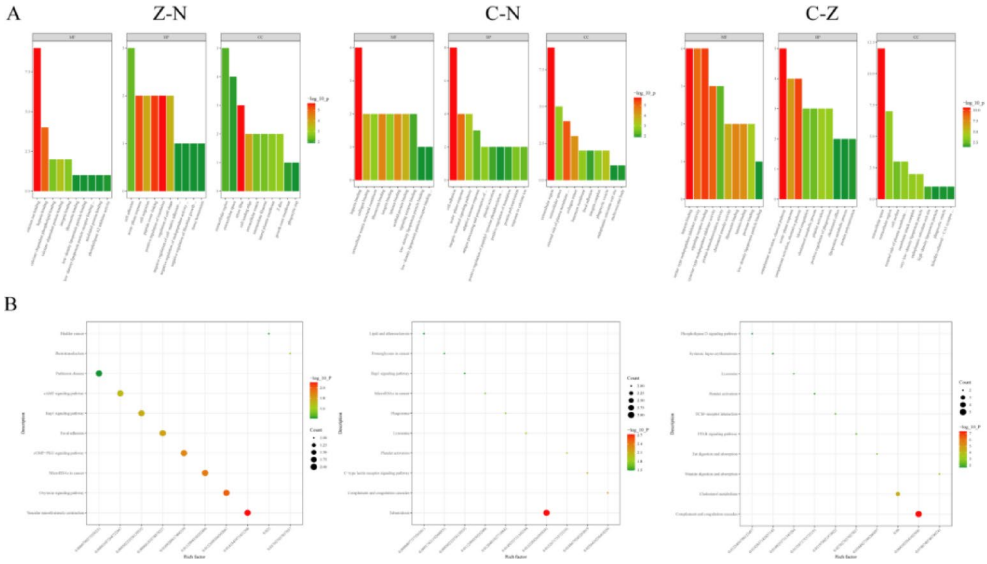

Fig. 7. GO and KEGG enrichment analysis of the top 30 DEPs. (**A**) GO terms enriched in GO enrichment analysis for the three comparison groups: C vs. N, C vs. Z, and Z vs. N. (**B**) Pathways enriched in KEGG enrichment analysis for the three comparison groups: C vs. N, C vs. Z, and Z vs. N.

Kyoto encyclopedia of genes and genomes (KEGG) pathway enrichment analysis

KEGG pathway enrichment analysis was conducted on the top 30 key proteins from each comparison group to identify enriched pathways. In the Z - N comparison group, key proteins were enriched in pathways such as Vascular smooth muscle contraction, Oxytocin signaling pathway, MicroRNAs in cancer, cGMP - PKG signaling pathway, Focal adhesion, Rap1 signaling pathway, and cAMP signaling pathway. The altered DEPs, including FN1, VIM, THBS1, FMOD, TIMP1, CCN2, MYH11, MYL9, and ANXA1, were involved in processes like angiogenesis, wound healing, cell adhesion, inflammation response, muscle contraction, and epithelial cell formation and differentiation. In the C - N comparison group, key proteins were enriched in pathways such as Complement and coagulation cascades, C - type lectin receptor signaling pathway, Platelet activation, Lysosome, Phagosome, Rap1 signaling pathway, and Proteoglycans in cancer. The altered DEPs, such as FN1, VIM, THBS1, FMOD, TIMP1, ITGB3, FGA, CTSS, CRP, HP, and COL1A2, participated in processes related to extracellular

matrix remodeling, angiogenesis, cell adhesion, and inflammation response. Proteases played a role in collagen degradation in the extracellular matrix, fibronectin facilitated protein polymerization, and LUM mitigated scar formation during regeneration, collectively regulating extracellular matrix remodeling. In the C - Z comparison group, key proteins were enriched in pathways such as Complement and coagulation cascades, Cholesterol metabolism, Vitamin digestion and absorption, Fat digestion and absorption, PPAR signaling pathway, ECM - receptor interaction, Platelet activation, and Lysosome. The altered DEPs, including PLG, FGA, HRG, HP, C3, C9, CRP, C5, C1Q1, ORM1, and SERPIND1, regulated complement activation, cell lysis, vascular endothelial growth factor production, lipid transport and metabolism, inflammation response, coagulation reaction, wound healing, vascular development, and extracellular matrix assembly (Fig. 7B). These analyses comprehensively illuminated the functional roles and pathways influenced by different bioengineered scaffolds during vaginal tissue regeneration.

Integration of mRNA and protein analysis

Transcriptomic and proteomic data were integrated in the analysis. Venn diagrams (Fig. 8A,B) showed the intersection of upregulated and downregulated genes and proteins in the N, Z, and C comparison groups. Correlation analysis revealed significant relationships between differentially expressed genes and proteins in these groups. Compared to the N group, the C group had 49 upregulated and 11 downregulated genes and proteins, while the Z group had 11 upregulated and 19 downregulated genes and proteins. Compared to the Z group, the C group had 48 upregulated and 19 downregulated genes and proteins. Correlation coefficient analysis (Fig. 8C) evaluated the relationship between differentially expressed proteins and genes. The heatmap indicated significant correlations between the selected differentially expressed proteins and genes, helping to understand how gene expression is regulated at both the mRNA and protein levels and shedding light on the molecular mechanisms of vaginal tissue regeneration.

GO enrichment analysis

GO enrichment analysis was performed on the differentially co - expressed genes and proteins from the comparisons between the N, Z, and C groups. Compared to the N group, the Z group's differentially co - expressed genes and proteins were mainly enriched in GO terms such as antioxidant activity, protein homodimerization, fibronectin binding, laminin binding, and hypotaurine dehydrogenase activity. They participated in biological processes including the immune system process, positive regulation of the transforming growth factor - beta receptor signaling pathway, cell adhesion, negative regulation of cell - matrix adhesion, negative regulation of the fibroblast growth factor receptor signaling pathway, and positive regulation of smooth muscle cell proliferation. These proteins were primarily localized in cellular components such as the actin cytoskeleton, bicellular tight junction, axon, endoplasmic reticulum membrane, brush border, cornified envelope, stress fiber, and ubiquitin ligase complex, potentially influencing immune responses, cell - cell and cell - matrix interactions, and smooth

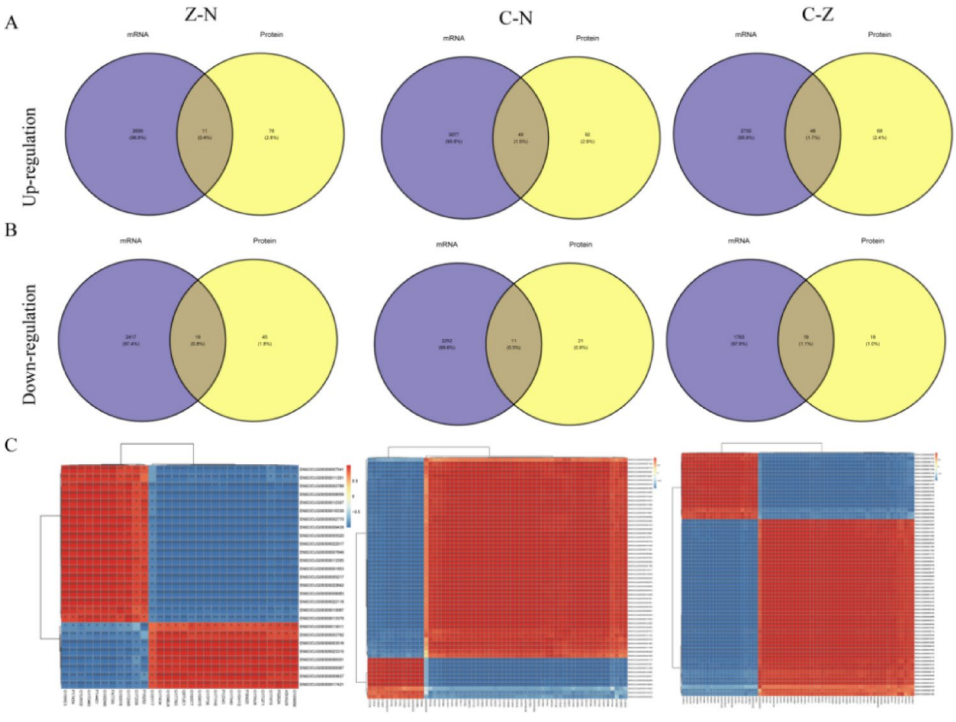

Fig. 8. (**A**) Venn diagram of upregulated genes and proteins in each comparison group, (**B**) Venn diagram of downregulated genes and proteins in each comparison group, (**C**) Heatmap showing the correlation between differentially expressed genes and proteins in each comparison group.

muscle proliferation. The differentially co - expressed genes and proteins in the C group, compared to the N group, were enriched in GO terms such as fibronectin binding, laminin binding, actin binding, calcium ion binding, hormone activity, misfolded protein binding, and antioxidant activity. They participated in biological processes such as the immune system process, camera - type eye development, positive regulation of the intrinsic apoptotic signaling pathway, positive regulation of protein kinase B signaling, regulation of cell population proliferation, and positive regulation of angiogenesis. These proteins were primarily localized in extracellular space, cornified envelope, cell - cell junction, skeletal muscle myofibril, cortical cytoskeleton, and myelin sheath, potentially regulating cell proliferation and apoptosis, angiogenesis, organ development, and inflammatory responses. Compared to the Z group, the differentially co - expressed genes and proteins in the C group were enriched in GO terms such as fibronectin binding, collagen binding, calmodulin binding, structural molecule activity, hormone activity, AMP - activated protein kinase activity, and antioxidant activity. They participated in biological processes including the cellular acute - phase response, inflammatory response, collagen catabolic process, vasoconstriction, cellular response to xenobiotic stimulus, glycogen catabolic process, positive regulation of the epidermal growth factor receptor signaling pathway, and ventricular cardiac muscle tissue morphogenesis. These proteins were significantly enriched in extracellular space, phagocytic cup, cell - cell junction, membrane raft, skeletal muscle myofibril, and protein folding chaperone complex, potentially influencing inflammation responses, extracellular matrix remodeling, vascular regeneration, and organ morphogenesis (Fig. 9A). This GO enrichment analysis revealed the functional roles and cellular processes affected by differentially expressed genes and proteins during vaginal tissue regeneration across the comparison groups.

KEGG pathway enrichment analysis

KEGG pathway enrichment analysis was conducted on the differentially co - expressed genes and proteins identified from the correlation analysis across the Z - N, C - N, and C - Z groups. In the Z - N group, these genes and proteins were significantly enriched in pathways such as leukocyte transendothelial migration, tight junctions, TGF - beta signaling, FoxO signaling, cell adhesion molecules, the renin - angiotensin system, taurine and hypotaurine metabolism, motor proteins, and focal adhesion. Key protein products involved, such as MYL9, THBS1, and HP, were associated with inflammation and immunity, vascular formation, cell - matrix interactions, tissue injury, and remodeling. In the C - N group, the differentially co - expressed genes and proteins were enriched in pathways including Phagosome, Glycolysis / Gluconeogenesis, p53 signaling pathway, Cytoskeleton in muscle cells, Fc gamma R - mediated phagocytosis, Natural killer cell mediated cytotoxicity, Protein digestion and absorption, and Renin - angiotensin system. Protein products such as CTSS, THBS1, COL8A1, and PYGM were identified, which were involved in inflammation and immunity, protein synthesis metabolism, cell proliferation, epithelial cell differentiation, endothelial formation, and embryonic organ morphogenesis. In the C - Z group, the differentially co - expressed genes or proteins were enriched in pathways such as Hypertrophic cardiomyopathy, Complement and coagulation cascades, Tight junction, Starch and sucrose metabolism, Cytoskeleton in muscle cells, PPAR signaling pathway, and Vascular smooth muscle contraction. Key protein products including MMP1, ORM1, and PYGM were highlighted, predominantly associated with cellular metabolism, immune response, extracellular matrix remodeling, and muscle organ morphogenesis (Fig. 9B). These KEGG pathway enrichment

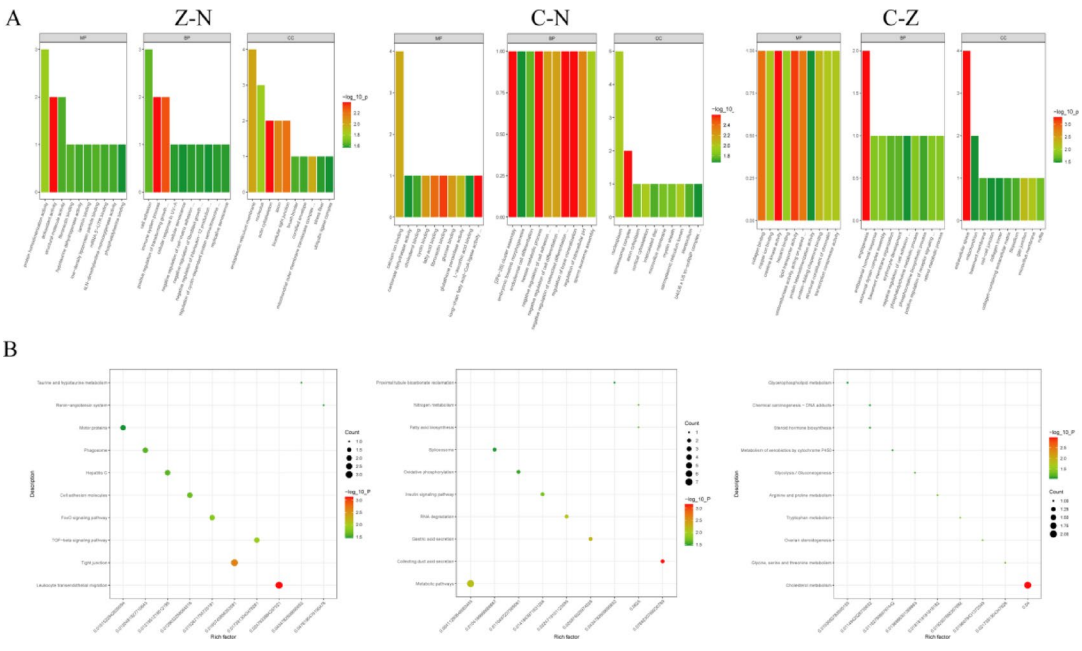

Fig. 9. GO and KEGG enrichment analysis for each comparison group includes: (**A**) Enriched GO terms for the three comparisons: C vs. N, C vs. Z, and Z vs. N, (**B**) Enriched pathways from KEGG analysis for the same comparisons: C vs. N, C vs. Z, and Z vs. N.

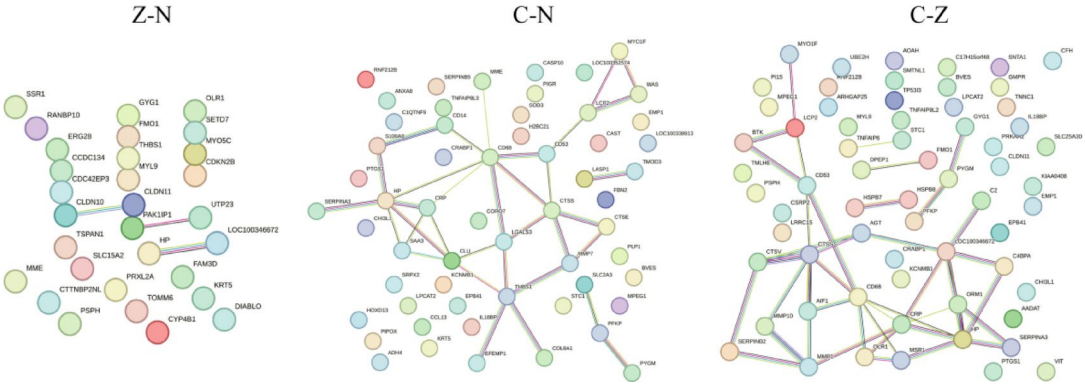

Fig. 10. PPI networks of differentially co-expressed genes and proteins for each comparison group: C vs. N, C vs. Z, and Z vs. N.

findings revealed the biological processes and molecular pathways affected by differentially expressed genes and proteins during vaginal tissue regeneration across the comparison groups.

PPI network analysis

The differentially co - expressed genes and proteins from the correlation analysis were visualized in the PPI network (Fig. 10). In the Z - N group, the protein corresponding to the HP gene occupied a central position in the network, mainly associated with oxidative stress and inflammatory responses. In the C - N group, proteins corresponding to the HP, CTSS, THBS1, CRP, and MMP7 genes were centrally located in the network. These proteins were predominantly involved in cellular metabolism, inflammation, and extracellular matrix remodeling. In the C - Z group, proteins corresponding to the CTSS, CRP, HP, MMP1, and ORM1 genes were central to the network. They were mainly associated with collagen degradation metabolism, vascular processes in the circulatory system, inflammation, and were implicated in cell proliferation, extracellular matrix remodeling, and immune responses. These key genes and proteins, located in the dense core regions of the network, interacted with each other and included many associated proteins. They collectively regulated organ development in animals and may be important targets for vaginal tissue regeneration.

Integrated analysis of results

In the Z group compared to N, 10 key upregulated proteins were identified: FN1, FMOD, VIM, THBS1, TIMP1, CCN2, MYH11, MYL9, and ANXA1, while HP was downregulated. In the C group compared to N, 14 key upregulated proteins were found: FN1, VIM, THBS1, FMOD, TIMP1, ITGB3, FGA, CTSS, CRP, HP, COL1A2, MMP7, COL8A1, with PYGM downregulated. In the C group compared to Z, 14 key upregulated proteins were identified: PLG, FGA, C9, CRP, C5, C3, C1Q1, ORM1, HRG, HP, MMP1, CTSS, SERPIND1, and PYGM was downregulated. TIMP1 was involved in cell proliferation through the HIF – 1, p53, and PI3K - Akt signaling pathways. THBS1 regulated cells via the Rap1 signaling pathway. MYL9 was linked to cell proliferation and vascular formation through the cAMP and oxytocin signaling pathways. These findings emphasized how the interactions among these proteins regulated vaginal tissue regeneration by influencing cellular.

Discussion

3D bioprinting technology holds great promise in the field of tissue repair and organ reconstruction. In the context of vaginal reconstruction, it offers personalized treatment options, a significant innovation that can closely mimic the natural morphology and function of the vagina[15]. The scaffold materials used in this technology possess excellent biocompatibility and bioactivity, enabling seamless integration with patient tissues and reducing the risks of rejection and infection. This not only enhances the safety of vaginal reconstruction surgeries but also improves their reliability[16]. Biomaterials play a crucial role in supporting cells, mimicking the extracellular matrix (ECM) structure and function, and promoting cell adhesion, proliferation, and differentiation[17]. When seed cells are incorporated into bioinks, they can differentiate into target cells such as epithelial and smooth muscle cells under specific conditions, facilitating tissue repair and regeneration and improving the local microenvironment for transplanted tissues[18,19]. In our study, we fabricated a novel ECM - GelMA - SF bioink using porcine vaginal tissue ECM and BMSCs and implanted it into rabbits for vaginal reconstruction. Macroscopic analysis demonstrated that all rabbits with the biomimetic scaffold had favorable vaginal structure and function. Moreover, scaffolds loaded with cells showed superior regenerative effects, indicating their efficacy in promoting vaginal regeneration. However, the mechanism underlying the role of 3D - printed biomimetic scaffolds in tissue reconstruction is complex, involving multiple levels of interaction and regulation[20]. Although mechanistic studies have been reported for other tissues like oral mucosa, glands, muscles, blood vessels, and neural tissue[21–24], the molecular mechanisms of 3D - printed biomimetic scaffolds in vaginal reconstruction remain unclear.

Building on our successful vaginal tissue construction, we employed combined transcriptomic and proteomic analyses. Transcriptomic analysis revealed a substantial number of differentially expressed genes in the 3D scaffold groups compared to the normal group. Specifically, there were 3,374 upregulated and 3,310

downregulated genes in the 3D scaffold group, and 4,023 upregulated and 3,226 downregulated genes in the 3D cell - loaded scaffold group. This difference might be attributed to the influence of BMSCs on gene expression regulation when loaded onto the scaffolds. Proteomic analysis further supported the transcriptomic findings. We identified key proteins involved in various aspects of vaginal regeneration, including inflammation, vascular formation, ECM remodeling, epithelial and muscle regeneration, neural regeneration, and glycogen synthesis. Additionally, scaffolds with stem cells were found to promote immune activation and coagulation during the regeneration process.

The tissue compatibility of biomaterials is intricately linked to the inflammatory response during tissue regeneration. A well - regulated inflammatory response can enhance the interaction between cells and materials and facilitate vascular formation. Vascularization is vital for tissue regeneration as it supplies nutrients and oxygen to new tissues. Moreover, neovascularization affects the migration of inflammatory cells, as new blood vessels can attract these cells, accelerating wound healing. In our study, we detected changes in inflammation - related proteins during vaginal reconstruction, such as CRP, THBS1, ANXA1, HRG, HP, ORM1, MYL9, and CTSS, along with their associated pathways. CRP, an acute - phase protein, is produced and released during infection or tissue injury. It directly regulates angiogenesis through the Wnt pathway and promotes liver cell regeneration both in vitro and in vivo[25]. Local inflammation at the wound site is essential for healing as it helps clear debris and protects against bacterial invasion. Fibroplasia and granulation tissue formation, along with epithelialization, contribute to the restoration of the protective skin layer[26]. However, excessive inflammation can cause further tissue damage and excessive scarring, so it must be strictly regulated and limited at the injury site.

THBS1, a multifunctional glycoprotein, is released by platelets, epithelial cells, and stromal cells during development, wound healing, angiogenesis, platelet aggregation, and cell adhesion. Without THBS1, inflammation can persist, wound healing may be delayed, and scab detachment can be slow[27]. Research has shown that THBS1 mRNA is undetectable in normal skin but present in early wounds, mainly sourced from macrophage - like cells in inflammatory infiltrates. Inhibiting THBS1 significantly delays wound repair by reducing re - epithelialization rates and slowing dermal remodeling, indicating that THBS1 produced by macrophages plays a crucial role in the repair process[28]. THBS1 works with angiogenic factors to control capillary angiogenesis and maintain vascular balance during regeneration[29]. These biological processes may involve signaling pathways such as Rap1, p53, and TGF - β. ANXA1, an anti - inflammatory protein mediated by glucocorticoids, reduces inflammation by inhibiting leukocyte activation and migration. It also regulates cell migration, promotes tissue repair, and is crucial for liver proliferation and regeneration[30]. In vivo, ANXA1 helps resolve inflammation by promoting wound closure and restoring epithelial barriers in intestinal cells[31]. Moreover, ANXA1 inhibits fibrosis gene expression, exhibits anti - fibrotic activity, promotes corneal epithelial wound healing, and reduces corneal inflammation[32]. The expression of HRG and CTSS was higher in the scaffold with stem cells compared to the scaffold alone. HRG, a liver - produced glycoprotein, regulates angiogenesis in both pro - and anti - angiogenic ways[33]. It reduces inflammation by inhibiting excessive neutrophil activation in circulation and protects the vascular endothelial barrier by regulating clotting pathways[34]. CTSS, a key cysteine protease, degrades anti - angiogenic peptides and adhesion proteins, promoting neovascularization, tumor cell invasion, and metastasis. CTSS degrades the endothelial basement membrane and promotes VSMC migration and proliferation through the p38MAPK/Akt signaling pathway, facilitating injury - related vascular repair[35,36]. Based on these findings, we hypothesize that stem cells may have a positive regulatory effect on inflammation and vascular formation. In summary, precisely regulating both pro - inflammatory and anti - inflammatory responses, as well as vascular formation, is of utmost importance throughout the vaginal regeneration process.

The ECM is a dynamic and flexible structure present in all tissues, providing support to cells and tissues and undergoing continuous and controlled changes. Our results indicated an upregulation of ECM remodeling - associated components in the scaffold group, including MMP1, MMP7, TIMP1, COL1A2, COL8A1, FMOD, FN1, VIM, and ITGB3. The breakdown of ECM components is a fundamental aspect of ECM remodeling, and matrix metalloproteinases (MMPs) play a crucial role in this process. MMP activity is typically low but increases during tissue repair, remodeling, and in diseased or inflamed tissues[37]. In our study, both bioengineered scaffolds for vaginal reconstruction showed a significant increase in MMPs (MMP − 1, MMP − 7) and higher levels of tissue inhibitors of metalloproteinases (TIMPs). MMPs are involved in various biological processes, such as tissue remodeling, growth, angiogenesis, tissue defense, and immune responses[38]. TIMPs usually regulate MMPs, and the balance between them determines the extent of ECM protein breakdown and tissue remodeling[39]. MMP1 helps assemble and repair the basement membrane, supporting wound re-epithelialization under oxidative stress and anti-fibrotic conditions[40,41].These findings suggest that MMP1 could be a potential anti-fibrotic agent for preventing or treating hypertrophic scars[42]. Angiogenesis requires the breakdown of the vascular basement membrane and ECM remodeling to enable endothelial cell migration into adjacent tissues. MMPs facilitate the actions of various angiogenic factors through their proteolytic activity, thereby promoting blood vessel formation[43]. However, MMPs may also exert anti - angiogenic effects by degrading specific collagen chains and plasminogen activators[44]. Overall, MMPs are important regulators of angiogenesis, generally promoting this process.

Collagen is the most abundant component of the ECM and is essential for tissue structure and function. Collagen fibers provide the framework for tissue shape, strength, and wound healing[45,46]. Type I collagen is the most prevalent type, found in blood vessels, cornea, sclera, tendons, ligaments, and skin, accounting for over 90% of ECM levels[47]. TIMP − 1 and COL1A1 work in tandem during the proliferation and remodeling stages of periodontal wound healing, playing a crucial role in preventing ECM and collagen breakdown during remodeling[48]. Collagen I interacts with different pro - fibrotic tissue remodeling proteins to form the ECM. Other ECM molecules, such as FN1 and TIMP − 1, integrate into this network to balance the construction and breakdown of damaged tissues[49]. COL8A1 is a secreted protein found in many rapidly growing cells and promotes

smooth muscle cell migration and proliferation during vascular remodeling[50]. The Col8a1 gene may serve as a biomarker for heart remodeling[51]. Endothelial - derived Col8a1 is a key factor in endothelial cell proliferation and may positively impact endothelial repair and the integrity of new intimal layers[52]. Fibronectin-1 (FN1) is a glycoprotein present on cell surfaces, in extracellular fluids, and in connective tissues. It interacts with collagens, fibronectins, and integrins, primarily supporting cell adhesion and being involved in cytoskeletal organization, cell migration, and important physiological processes like wound healing, thrombosis, and aging[53]. High levels of FN1 interact with integrin ITGB3, regulating gene activity that affects various signaling pathways and is involved in ovarian follicle development, maturation, ovulation, and corpus luteum formation[54]. During tissue injury, the mRNA levels of ITGB3 and FN1 increase under low - oxygen conditions, enabling them to accumulate locally, stimulate cell proliferation, accelerate blood vessel formation, and enhance wound healing[55]. The addition of stem cells further increases ITGB3 protein expression. Integrins are transmembrane receptors that help cells adhere to the ECM, bind to various growth factors, generate different intracellular signals, and regulate cell proliferation, differentiation, and fusion[56]. Phosphorylation of ITGB3 can stimulate angiogenesis and VEGF expression via the MAPK/ERK pathway, regulating vascular formation and stability[57].

Vimentin, a type III intermediate filament protein, is crucial for cell functions such as migration, proliferation, and division. It is also associated with cell adhesion and migration during epithelial - mesenchymal transition, ECM remodeling, and inflammatory responses, all of which are essential for normal wound healing[58]. Vimentin promotes nerve sprout growth and sensory recovery, providing neuroprotective functions[59]. Additionally, vimentin is essential for regulating vascular contraction, tension, endothelial integrity, and barrier function. It participates in vascular remodeling and smooth muscle cell differentiation, which are important for tissue homeostasis and repair[60]. Fibromodulin (FMOD) binds to ECM structural components, regulating collagen cross - linking, assembly, and fiber structure. It also interacts with signaling molecules, influencing cell adhesion, proliferation, migration, invasion, differentiation, and metastasis. Consequently, FMOD promotes migration, angiogenesis, anti - inflammation, and anti - fibrosis, playing significant roles in determining cell fate and tissue regeneration[61]. FMOD is involved in wound healing and the assembly of ECM components, such as collagen, and is closely related to muscle regeneration and myoblast proliferation and differentiation[62]. In adult wound models, FMOD can induce a more “fetal - like” migratory and contractile phenotype in adult dermal fibroblasts, reducing scar formation without compromising tensile strength[63]. During vaginal reconstruction, increased expression of collagen, fibronectin, and vimentin offers support and stability for new tissues, while MMPs, TIMPs, and FMOD aid in regeneration and repair by degrading and remodeling ECM components. The balance between these factors may be essential for successful vaginal tissue reconstruction.

We also observed an increased expression of CCN family members in the scaffold group. CCNs can promote tissue regeneration through various mediators, including growth factors, matrix proteins, and integrins[64]. For instance, CCN2 has been shown to accelerate the healing rate of burns and diabetic wounds[65,66]. It regulates keratinocyte migration, promoting re - epithelialization during skin wound healing[67]. The dynamic expression of CCNs during tissue regeneration drives epithelial regeneration and may mediate fibrogenesis and anti - fibrotic activity during repair. However, further research is needed to fully understand their dual regulatory mechanisms. FMOD may coordinate the spatiotemporal dynamics of TGF - β signaling through indirect mechanisms, such as modulating collagen cross - linking and ligand bioavailability, thereby regulating collagen fiber generation and potentially reducing scar formation in the extracellular matrix. In oral mucosal wound healing, the location and abundance of FMOD in the wound epithelium are regulated over time and space, promoting wound re - epithelialization and connective tissue regeneration[68]. The vagina, as a hollow organ, exhibits various contractile behaviors, such as peristalsis, tension maintenance, and spasms, due to its smooth muscle components. Beta – 3 integrin mediates myogenesis by regulating myogenic gene expression and satellite cell migration[69]. Myosin heavy chain subtype I (MYH1), part of the MYH gene family, encodes the MyHC - IIX protein, which is expressed in intermediate muscle fibers and contributes to the formation of skeletal muscle fibers[70,71]. MYH1 may be associated with SMSC differentiation and muscle fiber hypertrophy and is highly expressed in the late stages of C2C12 cell differentiation[70]. THBS1 promotes axon growth in neurons in vitro and aids axon regeneration in retinal ganglion cells through intrinsic mechanisms[72]. In addition, VIM, ITGB1 and CTSS can also regulate axon regeneration[73–75]. Vaginal epithelial cells produce glycogen, which is converted to lactate when shed, creating a unique microenvironment that inhibits the invasion of pathogenic bacteria[76]. In our study, we found that PYGM, a protein involved in glycogen breakdown metabolism, was downregulated in the reconstructed vaginal tissue with added cells. PYGM mainly provides energy for muscle contraction but is also expressed in other tissues and plays a key role in the early steps of glycogen breakdown through phosphorylation[77]. Inhibiting PYGM reduces glycogen breakdown, promoting glycogen storage within epithelial cells, which is beneficial for maintaining the vaginal microenvironment. The upregulation of CCN2, FMOD, MYH1, THBS1, VIM, and CTSS, along with the downregulation of PYGM, suggests that bioengineered scaffolds promote vaginal epithelialization, muscle regeneration, vaginal smooth muscle contraction, axon regeneration, and increased glycogen storage, facilitating the formation and recovery of vaginal tissue structure.

When comparing the cell - added group with the scaffold - only group, we found that the cell - added group had increased levels of proteins related to the coagulation cascade and anticoagulant systems, such as FGA, PLG, and SERPIND1, as well as proteins associated with the complement cascade and immune responses, including C9, C5, C3, C1Q1, HP, and ORM1. The coagulation, fibrinolysis, and complement systems are essential for maintaining tissue homeostasis. These cascades have numerous interactions that regulate fibrinolysis and complement activation during injury and acute inflammation[78]. Tissue injury, trauma, or systemic inflammation trigger the activation of the complement, coagulation, and fibrinolysis pathways. Despite their opposing functions, coordinated enzymatic cascades in these pathways repair damaged vessels and regulate the inflammatory process[79]. The final step of the coagulation cascade involves the conversion of fibrinogen alpha chain (FGA) to fibrin, which then polymerizes to form a blood clot[80]. Elevated FGA in inflammation - driven acute responses

promotes hemostasis by activating platelets, which help distribute red blood cells, macrophages, and fibroblasts around wounds. Controlling these processes is crucial for hemostasis, wound healing, and tissue regeneration[81]. Besides its role in hemostasis, FGA regulates leukocyte function during inflammation. Soluble fibrinogen influences neutrophil adhesion and affects leukocyte recruitment in vivo, thereby promoting inflammatory responses[82]. FGA and its degradation products also regulate vascular generation potential[83]. PLG is one of the most abundant proteins involved in hemostasis. It is activated by t - PA and u - PA to produce plasmin, which initiates fibrinolysis[84]. Plasminogen has functions beyond the fibrinolysis system, such as removing misfolded or aggregated proteins, triggering other enzyme cascades like complement activation, regulating cell behavior, and influencing immune and inflammatory processes. These functions enhance thrombolysis and accelerate wound repair[85]. FGA and PLG work in tandem to maintain the balance between the coagulation cascade and the fibrinolysis system, promoting tissue structure and functional reconstruction, especially in epithelial injury and reshaping[86]. The complement system is a key component of the innate immune system, serving as the first line of defense against invading pathogens. It also removes apoptotic and necrotic cells and regulates the adaptive immune system and inflammatory processes[87]. Complement has been shown to enhance coagulation by inhibiting fibrinolysis, while proteases from the coagulation and fibrinolysis systems cleave and activate C3 and generate C5a[88,89]. During infection, local complement - mediated coagulation activation enhances clotting, creating a barrier against bacterial spread and facilitating the production of antimicrobial peptides while supporting the inflammatory response[90]. In neovaginal formation, the coordinated action of the coagulation system, fibrinolysis system, and complement system is essential for maintaining tissue homeostasis. They ensure vascular integrity, prevent thrombus formation, resist foreign pathogens, and maintain tissue stability through precise regulation.

Conclusion

This study revealed the critical roles of genes and proteins related to extracellular matrix remodeling, vascular regeneration, inflammatory response, epithelialization, and muscle formation in vaginal reconstruction through combined transcriptomic and proteomic analysis. This research offers a new perspective on vaginal tissue regeneration and highlights the potential of personalized bio-scaffolds for promoting tissue repair and functional recovery. In the future, further exploration of these molecular mechanisms and improvements in 3D printing and cell therapy technologies aim to achieve better clinical outcomes.

Materials and methods

Experimental animals and grouping

Female New Zealand White rabbits aged 1–2 months, weighing 1.0–1.5 kg, were used to harvest BMSCs. Mature female New Zealand White rabbits aged 7–8 months, weighing 3.5–4.0 kg, were used to create a vaginal defect model for testing vaginal bioengineered scaffolds. All animals were bought from Tonghui Breeding Co., Ltd. in Wangdu County, Hebei Province, China. All procedures involving these animals strictly adhered to the Guidelines for Care and Use of Laboratory Animals of Hebei Medical University and received approval from the Animal Ethics Committee of the Second Hospital of Hebei Medical University(Approval Letter No.2024-AE011). All methods are reported in accordance with ARRIVE guidelines (https://arriveguidelines.org). Each animal was housed separately in the Animal Experimental Center of the Second Hospital of Hebei Medical University. There were three experimental groups: (1) Normal group ($n=4$): sham-operated group; (2) 3D cell-free biomimetic scaffold group ($n=4$): each rabbit received a bioengineered scaffold; (3) 3D cell-seeded biomimetic scaffold group ($n=4$): each rabbit received a scaffold seeded with rabbit BMSCs. Following the completion of the experiments, to ensure the comfort of the rabbits and alleviate their suffering, the researchers adhered to the guidance of the Animal Ethics Committee and employed euthanasia through overdose anesthesia. This method is considered a humane and effective means of euthanasia for experimental animals.

Preparation of BMSCs. Rabbit BMSCs were prepared by density gradient centrifugation and adherent culture. P3 cells were used for the experiments. When the cell fusion rate reached 80-90%, the cells were detached with trypsin and resuspended as a single-cell suspension for further use.

Preparation of vECM-GelMA-SF bioink

ECM was prepared as described previously[18]. The lyophilized ECM was ground into a powder and mixed with 3 ml of 0.01 mol/L HCl solution containing 45 mg of pepsin. Digestion was carried out at 37 °C, 80 rpm for 12 h to prepare vECM hydrogel. The pH was adjusted from acidic to neutral using 0.1 mol/L NaOH. GelMA (8% concentration) and photoinitiator (5%) were dissolved in 3 ml of sterile distilled water at 60 °C for 40 min, filtered through a 0.22 μm sterile filter, and sterilized by autoclaving. This solution was mixed with the prepared 3 ml vECM solution and 5% SF (50 mg/ml) to obtain vECM-GelMA-SF bioink. P3-BMSCs were added to the bioink at a concentration of $1\times10\text{^}7$ cells/ml, loaded into sterile syringes, and kept at 4 °C until use. The 3D biomimetic vaginal scaffold was printed using a JNOV Life 3D bioprinting system. An adapter needle (diameter 0.34 mm) was installed and fixed on the bioprinter's low-temperature nozzle. The scaffold parameters were set to X = 10 mm, Y = 10 mm, Z = 15 mm, with a layer thickness of 0.34 mm and 30 layers.

Biocompatibility testing of vECM-GelMA-SF bioink

P3-BMSCs loaded scaffolds were cultured in vitro for 7 days. Cell viability was assessed with a live/dead cell staining kit, and fluorescence confocal microscopy was used to observe cell survival.

Scaffold in situ transplantation

Experimental animals were anesthetized with 1% pentobarbital sodium (0.4 ml/100 g) via ear marginal vein injection. After anesthesia, the abdominal area was prepared and disinfected with iodine, and a midline incision was made in the lower abdomen to expose the uterus and vagina. Partial vaginal excision was performed by cutting the upper end of the vagina 5 mm below the cervix and the lower end 1 cm above the urethral meatus. The prepared bioengineered scaffold was fixed at the upper end to the external uterine orifice and aligned with the remaining vaginal end, then the abdominal cavity was closed layer by layer. All surgeries were performed by the same surgical team. To prevent infection, 1 million units of sodium penicillin were injected into the abdominal cavity once a day for 3 days.

Sample collection and evaluation

Three months post-surgery, newly formed vaginal tissues were collected for histological examination. The tissues were fixed in 4% paraformaldehyde, embedded in paraffin, and cut into 4 mm thick sections. Sections were stained with HE, Masson, VG, and PAS stains to observe epithelialization, vascularization, smooth muscle formation, and glycogen synthesis in the regenerated vaginal epithelium.

RNA sequencing

Vaginal tissues from the three groups, with three samples per group, were collected. Total RNA was extracted using TRIzol Reagent. RNA concentration and purity were assessed using an Agilent 2100 Bioanalyzer and RNA-specific agarose gel electrophoresis. mRNA enriched with polyA structure was selected using Oligo(dT) magnetic beads. RNA was then fragmented to approximately 300 bp using ion disruption, and 300 bp fragments were synthesized into cDNA using RNA as a template. After library construction, PCR amplification was performed to enrich the library fragments. Library size selection was set to 450 bp. The quality and concentration of the libraries were evaluated using the Agilent 2100 Bioanalyzer. The libraries were then subjected to next-generation sequencing (NGS) using the Illumina sequencing platform for paired-end (PE) sequencing.

DEGs analysis

Initially, the expression level correlation among samples was examined using Pearson correlation coefficien. PCA based on expression levels was conducted using the DESeq package in R. Differential gene expression analysis was performed using DESeq package in R. volcano plots were generated using ggplot2 package in R to display the distribution of genes, fold change differences, and significance results. DEGs specific to and shared among the comparison groups were statistically analyzed. Heatmaps were constructed using the pheatmap package in R to perform bidirectional clustering analysis of DEGs across all comparison groups, based on Euclidean distance and complete linkage method. DEGs were annotated using GO database (http://www.geneontology.org/) and GO annotation analysis was conducted using Goatools software. DEGs were also mapped to KEGG database (http://www.genome.jp/kegg/) for pathway enrichment analysis using KOBAS software[91–93].

Proteomic analysis

DIA analysis

Liquid chromatography-tandem mass spectrometry (LC-MS/MS) was used to identify peptide sequences ($n = 3$) from vaginal tissues of each group, which were then used for proteomic analysis. Adequate protein samples were used to construct a spectral library. Protein samples from each group were subjected to SDS-PAGE to assess sample consistency. Trypsin digestion was performed using FASP method. Peptide concentration was determined by OD280, and peptides were fractionated using HPRP method. Each fraction was analyzed by data-dependent acquisition (DDA) mass spectrometry after addition of iRT standard peptides. Nano-flow HPLC system Nanoelute was used for chromatographic separation. Peptides were analyzed by timsTOF Pro mass spectrometer after liquid chromatography separation. Maxquant software was used for data processing, and Mus musculus_uniprot database was employed for database searching with the following parameters: trypsin enzyme, maximum missed cleavage sites set to 2, fixed modification of Carbamidomethyl (C), and dynamic modifications of Oxidation (M) and Acetyl (Protein N-term). Identified proteins were filtered based on a false discovery rate (FDR) < 1%. Spectral libraries were constructed by importing raw files and search results into Maxquant software. DIA mass spectrometry was performed on all samples, with chromatographic separation using Nanoelute and the same liquid chromatography gradient and DDA testing conditions. Peptides separated by nano-flow high-performance liquid chromatography were analyzed by timsTOF Pro mass spectrometer using DIA data acquisition mode. Data were processed using Maxquant software with the same database used for library construction.

DEPs analysis

Annotation information corresponding to species was downloaded from uniprot. Direct and indirect interactions among DEPs were investigated based on STRING database (http://string-db.org/) information for PPI network analysis. Results from PPI network analysis were imported into Cytoscape (v3.7.1) to analyze and select proteins with top 30 Degree values. These proteins were further subjected to GO functional enrichment analysis and KEGG pathway enrichment analysis.

Integration analysis of transcriptomic and proteomic data

Transcriptomic and proteomic data were integrated to identify genes and proteins that were differentially expressed and regulated in the same way between the two sequencing methods. Venn diagrams were used to display the intersection of upregulated/downregulated genes and proteins. Correlation analysis was performed

to examine the relationship between differentially expressed proteins and genes. GO functional enrichment analysis and KEGG pathway enrichment analysis were conducted for differentially expressed genes and proteins. Direct and indirect interactions between differentially expressed genes and proteins were explored using STRING database, followed by PPI analysis to identify proteins with high connectivity.

Statistical analysis

GraphPad Prism 8.0 software was used for data processing. Continuous variables with a normal distribution were presented as mean ± standard deviation ($x \pm s$). Student's t-test was used to analyze the significance of differential gene and protein expression, with fold change (FC) criteria typically set at $p < 0.05$ and $FC > 2$ or < 0.5. GO and KEGG database analyses were conducted using Fisher's exact test for functional and pathway enrichment, with $p < 0.05$ indicating significant enrichment, where smaller values indicated more significant enrichment.

Data availability

Sequence data that support the findings of this study have been deposited in the NCBI with the primary accession code PRJNA1175434. Web Links：ID 1175434 - BioProject - NCBI.

Received: 24 September 2024; Accepted: 29 April 2025
Published online: 28 May 2025

References

1. McQuillan, S. K. & Grover, S. R. Dilation and surgical management in vaginal agenesis: a systematic review. *Int. Urogynecol. J.* **25** (3), 299–311 (2014).
2. Cheikhelard, A. et al. Surgery is not superior to dilation for the management of vaginal agenesis in Mayer-Rokitansky-Küster-Hauser syndrome: a multicenter comparative observational study in 131 patients. *Am. J. Obstet. Gynecol.* **219** (3), 281e1–281e9 (2018).
3. Brown, M. et al. Decellularized extracellular matrix: new promising and challenging biomaterials for regenerative medicine. *Biomaterials* **289**, 121786 (2022).
4. Fu, Z. et al. Injectable, stretchable, toughened, bioadhesive composite hydrogel for bladder injury repair. *RSC Adv.* **13** (16), 10903–10913 (2023).
5. Tutar, R. et al. Photocurable silk fibroin-based tissue sealants with enhanced adhesive properties for the treatment of corneal perforations. *J. Mater. Chem. B*. **10** (15), 2912–2925 (2022).
6. Brownell, D., Chabaud, S. & Bolduc, S. Tissue engineering in gynecology. *Int. J. Mol. Sci.* **23** (20). (2022).
7. Henckes, N. A. C. et al. Scaffold strategies combined with mesenchymal stem cells in vaginal construction: a review. *Cell. Regen*. **10** (1), 26 (2021).
8. Zhang, H. et al. The methods and mechanisms to differentiate Endothelial-Like cells and smooth muscle cells from mesenchymal stem cells for vascularization in vaginal reconstruction. *Mol. Biotechnol.* **60** (6), 396–411 (2018).
9. Wu, Y. et al. E2-Loaded microcapsules and bone Marrow-Derived mesenchymal stem cells with injectable scaffolds for endometrial regeneration application. *Tissue Eng. Part. A*. **30** (3–4), 115–130 (2024).
10. Kim, J. J. et al. Vascular regeneration and skeletal muscle repair induced by long-term exposure to SDF-1α derived from engineered mesenchymal stem cells after hindlimb ischemia. *Exp. Mol. Med.* **55** (10), 2248–2259 (2023).
11. De Francesco, F. et al. Artificial dermal substitutes for tissue regeneration: comparison of the clinical outcomes and histological findings of two templates. *J. Int. Med. Res.* **48** (8), 300060520945508 (2020).
12. Wang, H. & Sun, W. Q. Comparative proteomic analysis of regenerative acellular matrices: the effects of tissue source and processing method. *J. Biomed. Mater. Res. B Appl. Biomater.* **111** (12), 2002–2012 (2023).
13. McCabe, M. C., Saviola, A. J. & Hansen, K. C. Mass Spectrometry-Based atlas of extracellular matrix proteins across 25 mouse organs. *J. Proteome Res.* **22** (3), 790–801 (2023).
14. Ju, Y. et al. Extracellular vesicle-loaded hydrogels for tissue repair and regeneration. *Mater. Today Bio*. **18**, 100522 (2023).
15. Hou, C. et al. Printing 3D vagina tissue analogues with vagina decellularized extracellular matrix Bioink. *Int. J. Biol. Macromol.* **180**, 177–186 (2021).
16. Farzamfar, S., Richer, E. E., Chabaud, M., Naji, S. & Bolduc, M. S, Extracellular matrix-based and electrospun scaffolding systems for vaginal reconstruction. *Bioengineering (Basel)* **10** (7). (2023).
17. Peng, M., Wang, Z. Q. & Du, M. Reconfigurable scaffolds for adaptive tissue regeneration. *Nanoscale* **15** (13), 6105–6120 (2023).
18. Ma, Y., He, D. B. & Huang, R. Advancements of 3D Bioprinting in regenerative medicine: exploring cell sources for organ fabrication. *Heliyon* **10** (3), e24593 (2024).
19. Zhao, G. et al. Vaginal reconstruction by collagen scaffolds loaded with vaginal epithelial and smooth muscle cells in pigs. *Biomaterials Sci.* **12** (4), 1042–1054 (2024).
20. Wang, P., Shi, S. Y., Shen, X., Ning, H. & Liu, H. Bioscaffolds embedded with regulatory modules for cell growth and tissue formation: A review. *Bioact Mater.* **6** (5), 1283–1307 (2020).
21. Izumi, K. et al. Recent trends and perspectives in reconstruction and regeneration of intra/extra-oral wounds using tissue-engineered oral mucosa equivalents. *Jpn Dent. Sci. Rev.* **59**, 365–374 (2023).
22. Wang, T. et al. Injectable decellularized extracellular matrix hydrogel promotes salivary gland regeneration via endogenous stem cell recruitment and suppression of fibrogenesis. *Acta Biomater.* **169**, 256–272 (2023).
23. Hwangbo, H. et al. Bio-printing of aligned GelMa-based cell-laden structure for muscle tissue regeneration. *Bioact Mater.* **8**, 57–70 (2022).
24. Xue, C. et al. Skin derived precursors induced Schwann cells mediated tissue engineering-aided neuroregeneration across sciatic nerve defect. *Bioact Mater.* **33**, 572–590 (2024).
25. Jun, J. H., Kim, J. J., Hwang, J. Y., Bae, S. G. & Kim, S. H. Upregulation of C-Reactive protein by Placenta-Derived mesenchymal stem cells promotes angiogenesis in A rat model with cirrhotic liver. *Int. J. Stem Cells*. **13** (3), 404–413 (2020).
26. Greenhalgh, D. G. The role of apoptosis in wound healing. *Int. J. Biochem. Cell. Biol.* **30** (9), 1019–1030 (1998).
27. Blanco-Mezquita, J. T., Hutcheon, A. E. & Zieske, J. D. Role of thrombospondin-1 in repair of penetrating corneal wounds. *Invest. Ophthalmol. Vis. Sci.* **54** (9), 6262–6268 (2013).
28. DiPietro, L. A. et al. Thrombospondin 1 synthesis and function in wound repair. *Am. J. Pathol.* **148** (6), 1851–1860 (1996).
29. Li, J. et al. Circulating fibrocytes stabilize blood vessels during angiogenesis in a paracrine manner. *Am. J. Pathol.* **184** (2), 556–571 (2014).
30. Zagoura, D. et al. Functional secretome analysis reveals Annexin-A1 as important paracrine factor derived from fetal mesenchymal stem cells in hepatic regeneration. *EBioMedicine* **45**, 542–552 (2019).

31. Leoni, G. et al. Annexin A1, formyl peptide receptor, and NOX1 orchestrate epithelial repair. *J. Clin. Invest.* **123** (1), 443–454 (2013).
32. Hui, Q. et al. Annexin A1 promotes reparative angiogenesis and ameliorates neuronal injury in ischemic retinopathy. *Curr. Eye Res.* **47** (5), 791–801 (2022).
33. Kassaar, O. et al. Crystal structure of histidine-rich glycoprotein N2 domain reveals redox activity at an interdomain disulfide Bridge: implications for angiogenic regulation. *Blood* **123** (12), 1948–1955 (2014).
34. Gao, S. et al. Histidine-rich glycoprotein ameliorates endothelial barrier dysfunction through regulation of NF-κB and MAPK signal pathway. *Br. J. Pharmacol.* **176** (15), 2808–2824 (2019).
35. Shi, G. P. et al. Deficiency of the cysteine protease cathepsin S impairs microvessel growth. *Circ. Res.* **92** (5), 493–500 (2003).
36. Wu, H. et al. Activity controls Injury-Related vascular repair in mice via the TLR2-Mediated p38MAPK and PI3K-Akt/p-HDAC6 signaling pathway. *Arterioscler. Thromb. Vasc Biol.* **36** (8), 1549–1557 (2016).
37. Bonnans, C. & Werb, C. J. Remodelling the extracellular matrix in development and disease. *Nat. Rev. Mol. Cell. Biol.* **15** (12), 786–801 (2014).
38. Rohani, M. G. & Parks, W. C. Matrix remodeling by MMPs during wound repair. *Matrix Biol.* **44–46** 113–21. (2015).
39. Haubner, F. et al. A Co-Culture model of fibroblasts and adipose Tissue-Derived stem cells reveals new insights into impaired wound healing after radiotherapy. *Int. J. Mol. Sci.* **16** (11), 25947–25958 (2015).
40. Stevens, L. J. & Page-McCaw, A. A secreted MMP is required for reepithelialization during wound healing. *Mol. Biol. Cell.* **23** (6), 1068–1079 (2012).
41. Choi, A. et al. Anti-fibrotic effect of human Wharton's jelly-derived mesenchymal stem cells on skeletal muscle cells, mediated by secretion of MMP-1. *Int. J. Mol. Sci.* **21** (17). (2020).
42. Keskin, E. S. et al. The effect of MMP-1 on wound healing and Scar formation. *Aesthetic Plast. Surg.* **45** (6), 2973–2979 (2021).
43. Gao, P. et al. Nonischemic cerebral venous hypertension promotes a pro-angiogenic stage through HIF-1 downstream genes and leukocyte-derived MMP-9. *J. Cereb. Blood Flow. Metab.* **29** (8), 1482–1490 (2009).
44. Bendrik, C., Karlsson, L. & Dabrosin, C. Increased endostatin generation and decreased angiogenesis via MMP-9 by Tamoxifen in hormone dependent ovarian cancer. *Cancer Lett.* **292** (1), 32–40 (2010).
45. Shahrajabian, M. H. & Sun, W. Mechanism of action of collagen and epidermal growth factor: A review on theory and research methods. *Mini Rev. Med. Chem.* **24** (4), 453–477 (2024).
46. Mienaltowski, M. J. et al. Basic structure, physiology, and biochemistry of connective tissues and extracellular matrix collagens. *Adv. Exp. Med. Biol.* **1348**, 5–43 (2021).
47. Li, H. et al. The p38 signaling pathway mediates the TGF-β1-induced increase in type I collagen deposition in human granulosa cells. *Faseb J.* **34** (11), 15591–15604 (2020).
48. Kornsuthisopon, C. et al. Autologous platelet-rich fibrin stimulates canine periodontal regeneration. *Sci. Rep.* **10** (1), 1850 (2020).
49. Walter, A. S. et al. Systematic review of molecular pathways in burn wound healing. *Burns* **49** (7), 1525–1533 (2023).
50. Li, X. et al. Effects of COL8A1 on the proliferation of muscle-derived satellite cells. *Cell. Biol. Int.* **42** (9), 1132–1140 (2018).
51. Nawrocki, M. J. et al. Transcriptomic profile of genes regulating the structural organization of porcine atrial cardiomyocytes during primary in vitro culture. *Genes (Basel)* **13** (7). (2022).
52. Bao, H. et al. Platelet-Derived extracellular vesicles increase Col8a1 secretion and vascular stiffness in intimal injury. *Front. Cell. Dev. Biol.* **9**, 641763 (2021).
53. Goossens, K. et al. Quantification of fibronectin 1 (FN1) splice variants, including two novel ones, and analysis of integrins as candidate FN1 receptors in bovine preimplantation embryos. *BMC Dev. Biol.* **9**, 1 (2009).
54. Kulus, J. et al. Transcriptomic profile of new gene markers encoding proteins responsible for structure of Porcine ovarian granulosa cells. *Biology (Basel)* **10** (11). (2021).
55. Mathew, S. A., Chandravanshi, B. & Bhonde, R. Hypoxia primed placental mesenchymal stem cells for wound healing. *Life Sci.* **182**, 85–92 (2017).
56. Wang, C. et al. The role of PDIA3 in myogenesis during muscle regeneration. *Exp. Mol. Med.* **52** (1), 105–117 (2020).
57. Cho, H. et al. Regulation of endothelial cell activation and angiogenesis by injectable peptide nanofibers. *Acta Biomater.* **8** (1), 154–164 (2012).
58. Coelho-Rato, L. S. et al. Vimentin at the core of wound healing. *Trends Cell. Biol.* **34** (3), 239–254 (2024).
59. Ridge, K. M. et al. Roles of vimentin in health and disease. *Genes Dev.* **36** (7–8), 391–407 (2022).
60. van Engeland, N. C. A. et al. Vimentin regulates Notch signaling strength and arterial remodeling in response to hemodynamic stress. *Sci. Rep.* **9** (1), 12415 (2019).
61. Zheng, Z., Granado, H. S. & Li, C. Fibromodulin, a multifunctional matricellular modulator. *J. Dent. Res.* **102** (2), 125–134 (2023).
62. Lee, E. J. et al. Fibromodulin and regulation of the intricate balance between myoblast differentiation to myocytes or adipocyte-like cells. *Faseb J.* **32** (2), 768–781 (2018).
63. Zheng, Z. et al. Fibromodulin reduces Scar formation in adult cutaneous wounds by eliciting a fetal-like phenotype. *Signal. Transduct. Target. Ther.* **2**, 17050 (2017).
64. Barkin, J. M. et al. Significance of CCNs in liver regeneration. *J. Cell. Commun. Signal.* **17** (2), 321–332 (2023).
65. Liu, L. D. et al. The repairing effect of a Recombinant human connective-tissue growth factor in a burn-wounded rhesus-monkey (Macaca mulatta) model. *Biotechnol. Appl. Biochem.* **47** (Pt 2), 105–112 (2007).
66. Henshaw, F. R. et al. Topically applied connective tissue growth factor/CCN2 improves diabetic preclinical cutaneous wound healing: potential role for CTGF in human diabetic foot ulcer healing. *J. Diabetes Res.* **2015**, 236238 (2015).
67. Kiwanuka, E. & Eriksson, J. J. Transforming growth factor B1 regulates the expression of CCN2 in human keratinocytes via Smad-ERK signalling. *Int. Wound J.* **14** (6), 1006–1018 (2017).
68. Honardoust, D., Larjava, E. A. & Häkkinen, H. Localization of small leucine-rich proteoglycans and transforming growth factor-beta in human oral mucosal wound healing. *Wound Repair. Regen.* **16** (6), 814–823 (2008).
69. Liu, H. et al. Beta3-integrin mediates satellite cell differentiation in regenerating mouse muscle. *Faseb J.* **25** (6), 1914–1921 (2011).
70. Schiaffino, S. Muscle fiber type diversity revealed by anti-myosin heavy chain antibodies. *Febs J.* **285** (20), 3688–3694 (2018).
71. Long, K. et al. Identification of enhancers responsible for the coordinated expression of myosin heavy chain isoforms in skeletal muscle. *BMC Genom.* **23** (1), 519 (2022).
72. Bray, E. R. et al. Thrombospondin-1 mediates axon regeneration in retinal ganglion cells. *Neuron* **103** (4), 642–657e7 (2019).
73. Chen, K. Z. et al. Vimentin as a potential target for diverse nervous system diseases. *Neural Regen Res.* **18** (5), 969–975 (2023).
74. Ma, H. Y. et al. The progression of intracerebral hemorrhage (ICH) is related to the expression of integrin B1 (ITGB1). *Chin. Neurosurg. J.* **7** (1), 14 (2021).
75. Oshima, E. et al. M2 macrophage-derived cathepsin S promotes peripheral nerve regeneration via fibroblast-Schwann cell-signaling relay. *J. Neuroinflammation.* **20** (1), 258 (2023).
76. Kwon, M. S. & Lee, H. K. Host and Microbiome interplay shapes the vaginal microenvironment. *Front. Immunol.* 13. (2022).
77. Migocka-Patrzałek, M. & Elias, M. Muscle glycogen phosphorylase and its functional partners in health and disease. *Cells* **10** (4). (2021).
78. Agarwal, V. et al. A novel interaction between complement inhibitor C4b-binding protein and plasminogen that enhances plasminogen activation. *J. Biol. Chem.* **290** (30), 18333–18342 (2015).
79. Perucci, L. O. et al. Crosstalk between the plasminogen/plasmin system and inflammation resolution. *J. Thromb. Haemost.* **21** (10), 2666–2678 (2023).

80. Vorjohann, S. et al. Hypodysfibrinogenaemia due to production of mutant fibrinogen alpha-chains lacking fibrinopeptide A and polymerisation knob 'A'. *Thromb. Haemost*. **104** (5), 990–997 (2010).
81. Vilar, R. et al. Fibrin(ogen) in human disease: both friend and foe. *Haematologica* **105** (2), 284–296 (2020).
82. de Vitorino, V. et al. Fibrinogen modulates leukocyte recruitment in vivo during the acute inflammatory response. *Clin. Hemorheol Microcirc*. **59** (2), 97–106 (2015).
83. Staton, C. A., Brown, N. J. & Lewis, C. E. The role of fibrinogen and related fragments in tumour angiogenesis and metastasis. *Expert Opin. Biol. Ther.* **3** (7), 1105–1120 (2003).
84. Napolitano, F. & Montuori, N. Role of plasminogen activation system in platelet pathophysiology: emerging concepts for translational applications. *Int. J. Mol. Sci.* **23** (11). (2022).
85. Keragala, C. B. & Medcalf, R. L. Plasminogen: an enigmatic Zymogen. *Blood* **137** (21), 2881–2889 (2021).
86. Coden, M. E. & Berdnikovs, S. Eosinophils in wound healing and epithelial remodeling: is coagulation a missing link? *J. Leukoc. Biol.* **108** (1), 93–103 (2020).
87. Holers, V. M. Complement and its receptors: new insights into human disease. *Annu. Rev. Immunol.* **32**, 433–459 (2014).
88. Markiewski, M. M. et al. Complement and coagulation: strangers or partners in crime? *Trends Immunol.* **28** (4), 184–192 (2007).
89. Huber-Lang, M. et al. Generation of C5a in the absence of C3: a new complement activation pathway. *Nat. Med.* **12** (6), 682–687 (2006).
90. Frick, I. M. et al. The contact system–a novel branch of innate immunity generating antibacterial peptides. *Embo J.* **25** (23), 5569–5578 (2006).
91. Kanehisa, M. & Goto, S. KEGG: Kyoto encyclopedia of genes and genomes. *Nucleic Acids Res.* **28** (1), 27–30. https://doi.org/10.1093/nar/28.1.27 (2000).
92. Kanehisa, M. Toward Understanding the origin and evolution of cellular organisms. *Protein Sci.* **28** (11), 1947–1951. https://doi.org/10.1002/pro.3715 (2019).
93. Kanehisa, M., Furumichi, M., Sato, Y., Kawashima, M. & Ishiguro-Watanabe, M. KEGG for taxonomy-based analysis of pathways and genomes. *Nucleic Acids Res.* **51** (D1), D587–D592. https://doi.org/10.1093/nar/gkac963 (2023).

Acknowledgements

We extend our gratitude to all members of the Hebei Key Laboratory of Regenerative Medicine of Obstetrics and Gynecology and Hebei Medical University's Core Facilities and Centers for their valuable discussions regarding this work and the manuscript. The authors extend their gratitude to technicist from Shiyanjia Lab (www.shiyanjia.com) for the sequencing services and bioinformatic analysis.

Author contributions

Xuemei Zhang and Jiahua Zheng, contributed to conception, design, acquisition, analysis, and interpretation of data, drafed manuscript, revised manuscript. Xianghua Huang and Lin Zhang, contributed to acquisition, analysis, and interpretation of data, critically revised manuscript, gave fnal approval. Liye Zhang and Jingkun Zhang, acquisited and analyzed the datas. Li Feng, critically revised manuscript. All authors edited and approved the final manuscript.

Declarations

Competing interests

The authors declare no competing interests.

Additional information

Correspondence and requests for materials should be addressed to L.Z. or X.H.